

# Progress in the Puck Failure Theory for Fibre Reinforced Composites: Analytical solutions for 3D-stress

Alfred Puck <sup>a,\*</sup> and H. Matthias Deuschle <sup>b,\*\*</sup>

<sup>a</sup> Am Ahlberg 33, 34376 Immenhausen, Germany.

<sup>b</sup> KOLT Engineering GmbH, Schickardstraße 32, 71034 Böblingen, Germany.

\* Corresponding author regarding application. Tel.: +49-7031-79385-33; fax: +49-7031-79385-77, *Email*: [matthias.deuschle@gmx.de](mailto:matthias.deuschle@gmx.de) (H. Matthias Deuschle).

\*\* Corresponding author regarding Failure Theory. Tel.: +49-5673-3517; fax: +49-5673-3517, *Email* [alfred.puck@gmx.de](mailto:alfred.puck@gmx.de) (A. Puck)

## Abstract

The Puck fracture criteria for unidirectional fibre/polymer composites are widely accepted for physically based prediction of failure and post-failure degradation behaviour. The core of the theory, the inter-fibre fracture criteria, are criteria of the Coulomb/Mohr type. Accordingly, the inclination of the fibre-parallel fracture plane – in other words: the fracture angle – has to be determined in the first analysis step. Afterwards the fracture stresses acting on the predicted fracture plane can be determined. Since the theory has first been introduced continuous efforts have been taken to reduce the computational cost of such two-step approach. Since 1996 a closed analytical solution has been available for in-plane loadcases including  $(\sigma_1, \sigma_2, \tau_{21})$ -stress combination which are dominant in thin shells. During the authors' participation in the World Wide Failure Exercise II now an analytical solution for triaxial  $(\sigma_1, \sigma_2, \sigma_3, \tau_{23})$ -stress combinations has been derived. This paper presents closed analytical solutions for fracture angles, fracture stresses and stress exposure ratios useful for an efficient design process. Additionally, the understanding of intrinsically brittle fracture has been significantly improved and a mathematically and mechanically consistent classification of brittle behaviour is provided.

*Key words: Failure prediction, fibre reinforced composites, analytical solution*

**This document is available online at [www.alfredpuck.de](http://www.alfredpuck.de)**

## Notation

$x, y, z$	Global coordinate system of a laminate
$x_1, x_2, x_3$	Coordinate system of a UD lamina, $x_1$ being fibre-parallel, $x_3$ in through-thickness direction
$x_{\parallel}, x_{\perp}$	Cylindrical coordinate system of a UD lamina, $x_{\parallel}$ being fibre-parallel
$x_1, x_n, x_t$	Coordinate system of an action plane, $x_1$ being fibre-parallel
$c$	Index denoting compression
$f$	Index denoting fibres/ figures
$f_E$	Stress exposure
$f_S$	Stretch factor
$fr, fp$	Index denoting fracture / fracture plane
$FF, IFF$	Index denoting figures concerning fibre fracture / inter-fibre fracture
$m_{\sigma_f}$	Magnification factor for matrix and transverse fibre stresses
$p$	Inclination parameter
$R$	Strength of the material
$R^A$	Fracture resistance of the action plane
$t$	Index denoting tension
$\delta$	Angle difference, see Fig. 7
$\theta$	Angle between an arbitrary action plane and the action plane of $\sigma_2$
$\Theta$	Angle between an arbitrary action plane and the action plane of $\sigma_{II}$
$\sigma$	Normal stress
$\tau_{ij}$	Shear stress. Designation: first index represents normal to action plane and the second represents the direction of the shear stress

### Designation of Stresses

shear stresses  $\tau_{ab}$ :  
**a** defines the normal of the action plane  
**b** defines the shear stress direction

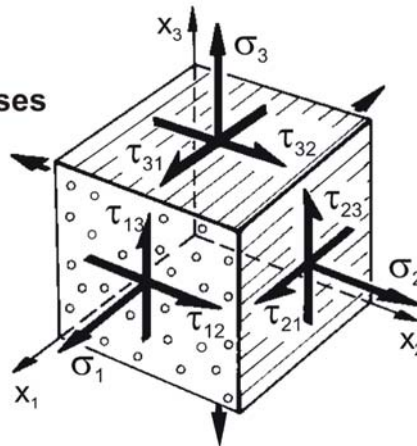


Fig. 1: Definition of the 3D direct and shear stresses in a UD lamina.

# 1 Introduction

Engineering composite materials have been the subject of interest in academia and industry for several decades. However, it is only recently that they started replacing conventional materials in primary structural assemblies. For instance, large rotor blades made of composites are being built for offshore wind turbines around Europe [1]. The Airbus A380's wing box, being the most important part for transferring the load between the wings and the fuselage, is made of fibre reinforced composite (FRC) materials [2]. Also, the dreamliner' Boeing 787, currently entering service, is the first large civil airliner where the main structures of the fuselage, the wings and the tail units are made of carbon/epoxy (CFRP) composites.

These great advances have been made possible by huge progress in manufacturing techniques as well as the massive increase of computing power in the last two decades. Along with being able to use more complex models, the components which can be studied to predict the failure behaviour can also be a lot more detailed. Based on the growing reliability of in-plane failure prediction [3] the application of FRC has been extended to complex geometries including primary load transferring components, resulting occasionally in 3D loading of the material. A safe design of such materials and structures requires an efficient and reliable failure prediction under general 3D states of stress. In that sense, the Puck Failure Theory has proven to meet highest demands and is inherently three-dimensional already from the beginning of its development [4].

The present paper starts with a brief overview of Puck's fibre and inter-fibre fracture criteria (see Sec. 2). Newly derived analytical solutions are then presented for some typical three dimensional fracture analysis problems (see Sec. 3) and for the parameter determination in case of non-intrinsically brittle material (see sec. 4).

## 2. Essentials of the Puck Fracture Theory

### 2.1 Historical background

Half a century ago, in March 1961, a comparatively small sailplane designed by Alfred Puck was launched into the air by a group of German students at the Darmstadt Technical University [5]. Surprisingly, in spite of its low span length of 12.6m, the DARMSTADT D-34d was able to compete with more sophisticated and expensive sailplanes having 18m span length. This has been achieved by an extraordinary smooth and accurate surface of the wing which featured a new low drag 'laminar profile'. It was the first time that the skin of a sailplane wing was designed as a pure shell structure made of  $0^\circ/\pm 45^\circ$  GFRP laminate (5mm thick at the fuselage and 2mm at the wing tip). The thin shell structure was filled with a stiff but very light honeycomb core to prevent buckling [5]. The success achieved in the design of those early composite structures is the basis and of a great significance for the present work. Students of the technical universities of Stuttgart and Brunswick were also working on high performance composite sailplanes. Thus, in the 1960s and 1970s, there was a strong competition in this field. As a result, a small but successful industrial section began to develop and build composite sailplanes. Since then and

over the years, Germany established a leading position in the worldwide supply of high performance GFRP and CFRP sailplanes [6].

In the following some of the early sailplane designers became involved in research and development of composite theory both in academic and commercial projects. Puck has been a member of the German Plastics Institute at Darmstadt from 1960 to 1970. Together with H. Wurtinger he published papers on GFRP design and dimensioning of GFRP-components [7, 8]. Obviously, the sailplane design activities had a strong influence on the development of a ‘German style of composite theory’. This influence can also be found in Puck’s failure theory until now. It successfully combines the practical aspects of an *engineering* theory with the scientific approach of a *material science* theory. The philosophy behind this approach follows the dictum that one should understand and be able to answer the following three questions:

- (a) *Why does damage or failure take place?*
- (b) *What happens during failure?*
- (c) *How can failure be avoided and what measures should be taken to achieve that?*

Already in his early phase of sailplane design Puck realised that fibre failure (FF) and inter-fibre failure (IFF) must be treated by different criteria. Back in 1969 a simple maximum stress failure condition for FF has been published [9,10]:

$$\frac{\sigma_1}{R_{\parallel}^t} \quad \text{for } \sigma_1 > 0 \quad (1)$$

and

$$\frac{\sigma_1}{(-R_{\parallel}^c)} \quad \text{for } \sigma_1 < 0 \quad (2)$$

## 2.2 Refinement of the fibre failure criterion

We shall now investigate the question of possible influence of transverse stresses on the longitudinal stress at fracture. As long as additional stresses  $\sigma_2$ ,  $\sigma_3$ ,  $\tau_{23}$ ,  $\tau_{31}$  and/or  $\tau_{21}$  remain about one order of magnitude lower than  $\sigma_1$  the simple criteria in Eqs. 1 and 2 are sufficient. However, if  $\sigma_2$  and/or  $\sigma_3$  reach values comparable to  $\sigma_1$ , this fibre-perpendicular stresses will have a direct effect on FF, which should be taken into account.

Due to the different Poisson’s ratios of fibre and matrix ( $\nu_{\parallel\perp f}$  and  $\nu_{\parallel\perp m}$ , respectively) the fibre-perpendicular stresses produce internal stresses  $\sigma_{1f}^i$  and  $\sigma_{1m}^i$  in the fibre direction. The term *internal* refers to the fact that  $\sigma_{1f}^i$  and  $\sigma_{1m}^i$  compensate each other and are not associated with any additional external load. Depending on the applied loads, the  $\sigma_{1f}^i$  either increases or decreases the fibre-parallel tension or compression effective in the fibres and has an influence on the IFF accordingly. We therefore have developed a more refined FF-condition on the following fracture hypothesis [6,7,8]:

Fibre fracture of a UD-composite under combined stresses will occur when in the fibres the same longitudinal stress  $\sigma_{1f}$  is reached which is acting in the fibres at an FF of the UD-composite caused by uniaxial tensile stress  $\sigma_1^t$  or a uniaxial compressive stress  $\sigma_1^c$ , respectively.

This means that fibre-failure prediction of a UD-composite should rather be based on the longitudinal stresses effective in the fibre  $\sigma_{1f}$  than on the fibre-parallel stress  $\sigma_1$  of the composite.

The following considerations are based on the fact that fibres and matrix experience the same strain in fibre direction under any loadcase. Under *uniaxial* stress  $\sigma_1$  of the composite, the stress  $\sigma_{1f}^{fr}$  in the fibres at fracture of the UD-composite is given as:

$$\sigma_{1f}^{fr} = E_{\parallel f} \frac{\pm R_{\parallel}^{t/c}}{E_{\parallel}} \quad (3)$$

At FF under *three-axial stress* ( $\sigma_1, \sigma_2$  and  $\sigma_3$ ) the longitudinal strain in the fibres is equal to that of the whole UD-composite:

$$\frac{\sigma_{1f}^{fr}}{E_{\parallel f}} - \frac{\nu_{\parallel f}}{E_{\perp f}} \cdot m_{\sigma_f} \cdot (\sigma_2 + \sigma_3) = \frac{\sigma_1^{fr}}{E_{\parallel}} - \frac{\nu_{\parallel}}{E_{\perp}} \cdot (\sigma_2 + \sigma_3) \quad (4)$$

$m_{\sigma_f}$  is the medium stress magnification factor of the transverse stress in the fibres due to the inhomogeneity of the stress acting in the UD-composite in the transverse direction (see Fig. 2). Estimated values for  $m_{\sigma_f}$  are 1.1 for CFRP and 1.3 for GFRP.

Using  $\frac{\nu_{\parallel f}}{E_{\perp f}} = \frac{\nu_{\perp \parallel f}}{E_{\parallel f}}$  and  $\frac{\nu_{\parallel}}{E_{\perp}} = \frac{\nu_{\perp \parallel}}{E_{\parallel}}$ , the fibre parallel stress at fracture  $\sigma_{1f}^{fr}$  follows from Eq. 3 and Eq. 4:

$$\sigma_{1f}^{fr} = \pm R_{\parallel}^{t/c} + \left( \nu_{\perp \parallel} - \nu_{\perp \parallel f} \frac{E_{\parallel}}{E_{\parallel f}} m_{\sigma_f} \right) (\sigma_2 + \sigma_3) \quad (5)$$

$\frac{E_{\parallel}}{E_{\parallel f}}$  can be replaced approximately by the volume fibre fraction,  $V_f$ , of the composite. Obviously, the magnitude of the sustainable longitudinal stress  $\sigma_{1f}^{fr}$  increases if the term  $(\sigma_2 + \sigma_3)$  has the same sign as  $\sigma_1$  and decreases if they have opposite signs.

One could imagine that constant radial compression as produced by hydrostatic pressure could impede kinking [11]. This should be investigated more thoroughly.

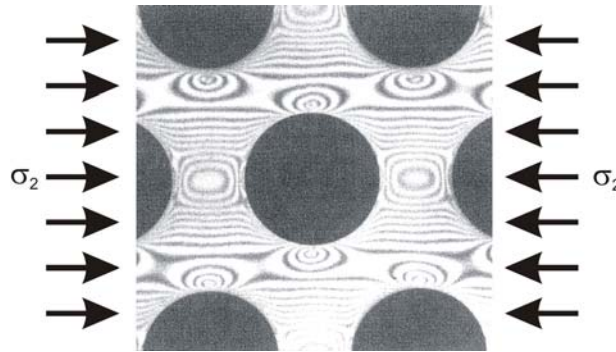


**Fig 2: Isochromatic lines in an epoxy plate with embedded aluminium rods demonstrate stress magnification in those areas where transverse compressive load has to be transferred through a chain of ‘soft’ resin area and stiff ‘fibre’ areas. (photo by Puck, German Plastics Institute, Darmstadt, 1968).**

Remains the question if  $\tau_{21}$  and/or  $\tau_{31}$  shear stresses also influence the fibre-parallel strength  $R_{\parallel}$ . In this context it is worthwhile noting the results of recent experimental research at the Institute for Plastic Processing in Aachen regarding whether or not there is any influence of  $\tau_{\perp\parallel}$ -shear stressing on the longitudinal strength  $R_{\parallel}$  [12].

There appears to be a quite remarkable linear weakening effect of  $\tau_{\perp\parallel}$ -shear stressing on the longitudinal compressive stress  $\sigma_1^{c\ fr}$  (see. Fig. 3). However, these are preliminary results and it is important to conduct further work in this area before a reliable trend is established.

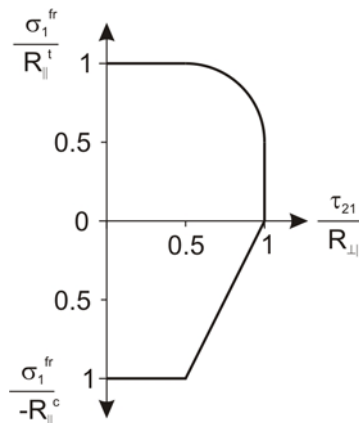


**Fig 3: Influence of  $\tau_{\perp\parallel}$ -stressing on longitudinal strength of UD-carbon/epoxy composite [12].**

### 2.3 Fundamental features of the theory of inter-fibre failure

During the 1960s and 70s a vast number of experiments involving various specimens and components have been conducted. It has been observed that a large number of inter-fibre fractures occur in the form of small brittle cracks long before the complete

disintegration of the component [10]. After investigating and assessing various theoretical approaches we are now convinced that the ideas of Coulomb [13] and Mohr [14] concerning brittle fracture should be the key to realistically and physically based IFF fracture criteria, dealing with transversally isotropic fibre matrix composites [14,15]. From the beginning it was obvious that this approach requires additional computing time for the calculation of the fracture angle. However, structural engineers will certainly be willing to put in more computational effort in order to achieve a higher degree of reliability. For the last couple of years continuous efforts have been taken to minimize this additional effort.

In brittle fractures macroscopically smooth fracture planes suddenly appear without any preceding major local deformations. Coulomb and later Mohr have come to the conclusion that such nearly smooth spontaneous fractures result from the tensile and /or shear stresses on the fracture surface at the moment of fracturing. They have also found that if a shear stress and a compressive stress are acting on the fracture surface simultaneously, the shear stress required for producing the fracture increases with increasing compressive stress. These fundamental hypotheses have been transferred to transversally isotropic fibre matrix composites by the Puck fracture criteria.

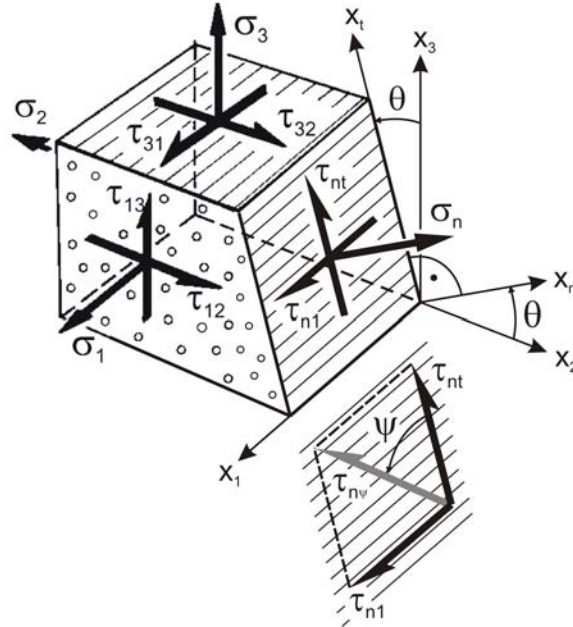


**Fig. 4: Definition of stresses  $\tau_n$ ,  $\tau_{nt}$ ,  $\tau_{n1}$  on a fibre parallel plane which is inclined to the action plane of stress  $\sigma_2$  by an angle  $\theta$ .**

Unlike in isotropic materials two shear stresses have to be considered for a fibre-parallel plane, since their different directions in relation to the direction of the fibres  $x_1$  are of importance for the micro-mechanical fracture process. We find a shear stress  $\tau_{nt}$  causing a  $\tau_{\perp\perp}$ -stressing and a shear stress  $\tau_{n1}$  causing a  $\tau_{\perp\parallel}$ -stressing (see Fig. 4). In order to point out the analogy to the Coulomb/Mohr theory, the two shear stresses – since they have the same action plane – can be replaced by their resultant [4]:

$$\tau_{n\psi} = \sqrt{\tau_{nt}^2 + \tau_{n1}^2} \quad (6)$$

Thus the fracture hypothesis for inter fibre fracture (IFF) is described as follows:

*Inter Fiber Fracture on a plane parallel to the fibers is governed by the stresses  $\sigma_n$  and  $\tau_{n\psi}$  acting on the fracture plane.*

*If  $\sigma_n$  is a tensile stress it promotes fracture together with the shear stress  $\tau_{n\psi}$  or even alone if  $\tau_{n\psi} = 0$ . In contrast to that  $\sigma_n$  impedes fracture if it is a compressive stress by raising the fracture resistance of the fracture plane against shear fracture with increasing compressive stress  $\sigma_n$ . A uniaxial compressive stress alone cannot produce a fracture of its action plane.*

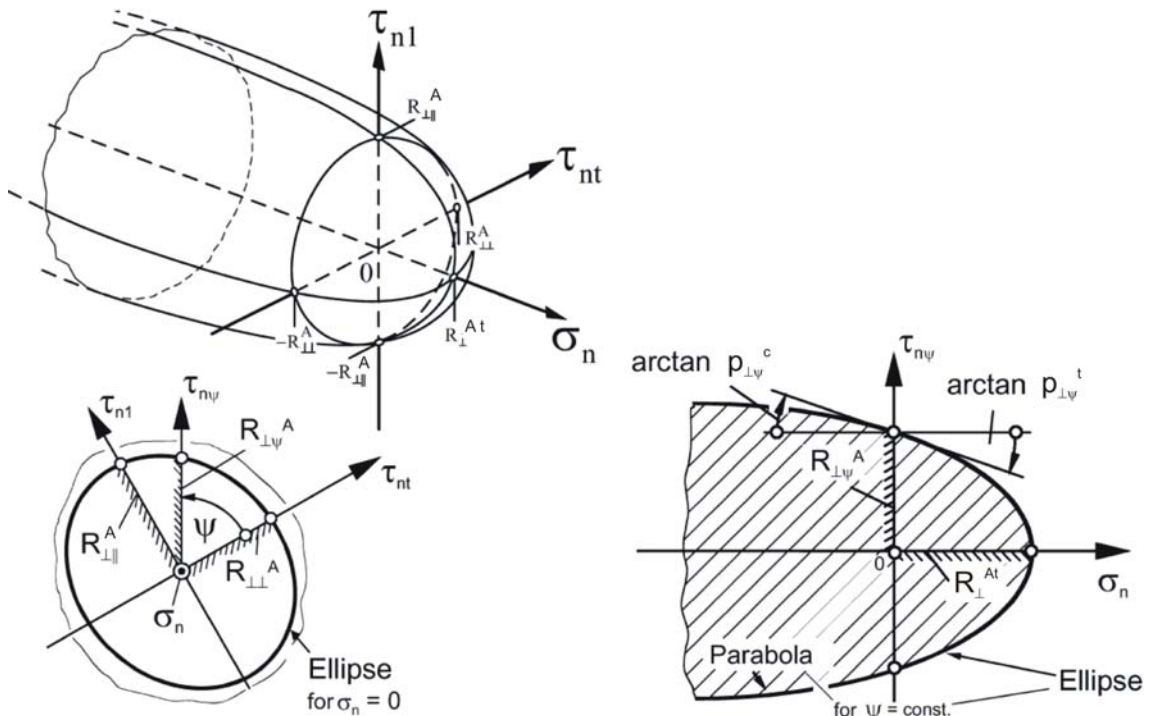


**Fig. 5: Master Fracture Body of the Puck inter-fibre fracture criterion.**

When accepting an astonishingly simple fracture hypothesis on the Coulomb/Mohr basis, one must also accept the associated considerations regarding the adequate *strengths* which might appear unusual. Fracture criteria for combined stresses always need some anchor points obtained in tests with simple loading conditions. For conventional failure criteria which are often pure interpolation polynomials, tensile strength, compressive strength, longitudinal shear strength, e.g., are used as experimentally accessible anchor points. They are the points where the failure envelope intersects the coordinate axes of the applied stress space. The situation is quite different if we try to formulate action plane related fracture criteria of the Coulomb/Mohr type. Starting from the hypothesis that the stresses  $\sigma_n^t$ ,  $\tau_{nt}$  and  $\tau_{n\parallel}$  representing a  $\sigma_{\perp}^t$ -,  $\tau_{\perp\perp}$ - and  $\tau_{\perp\parallel}$ -stressing in the lamina coordinate system, provoke the fracturing of the joint action plane, the following question arises regarding the anchor points of the respective fracture envelope: To which value of  $\sigma_{\perp}^t$  or  $\tau_{\perp\perp}$  or

$\tau_{\perp\parallel}$  has each of the stressings in a uniaxial tensile or a pure shear test to be increased in order to produce a fracture of the action plane? Thus, for a fracture criterion related to the action plane of the stresses, one has to use *fracture resistances*  $R^A$  of the *action plane* as opposed to the conventional *strengths*  $R$  [4]. The fracture resistances of the action plane are defined as follows:

*A fracture resistance of the action plane is the resistance (expressed in the dimension of a stress) by which an action plane resists its own fracture by a single stressing ( $\sigma_{\perp}^t$  or  $\tau_{\perp\perp}$  or  $\tau_{\perp\parallel}$ ) acting in the action plane under consideration. Corresponding to the three stressings, there are three fracture resistances of the action plane, namely  $R_{\perp}^{At}$ ,  $R_{\perp\perp}^A$ ,  $R_{\perp\parallel}^A$ .*

$$\begin{array}{c}
 \text{For the plane } \tau_{n1}=0 \\
 \left. \begin{array}{l} \text{for } \sigma_n \leq 0 \\ (\tau_{nt})^2 = \left(R_{\perp\perp}^A\right)^2 - 2p_{\perp\perp} R_{\perp\perp}^A \sigma_n \end{array} \right| \begin{array}{l} \text{for } \sigma_n \geq 0 \\ (\tau_{nt})^2 = \left(R_{\perp\perp}^A\right)^2 - 2p_{\perp\perp} R_{\perp\perp}^A \sigma_n - \left[ \left(\frac{R_{\perp\parallel}^A}{R_{\perp}^{At}}\right)^2 - 2p_{\perp\parallel} \frac{R_{\perp\parallel}^A}{R_{\perp}^{At}} \right] \sigma_n^2 \end{array} \\
 \text{For the plane } \tau_{nt}=0 \\
 \left. \begin{array}{l} \text{for } \sigma_n \leq 0 \\ (\tau_{n1})^2 = \left(R_{\perp\parallel}^A\right)^2 - 2p_{\perp\parallel}^c R_{\perp\parallel}^A \sigma_n \end{array} \right| \begin{array}{l} \text{for } \sigma_n \geq 0 \\ (\tau_{n1})^2 = \left(R_{\perp\parallel}^A\right)^2 - 2p_{\perp\parallel}^t R_{\perp\parallel}^A \sigma_n - \left[ \left(\frac{R_{\perp\parallel}^A}{R_{\perp}^{At}}\right)^2 - 2p_{\perp\parallel}^t \frac{R_{\perp\parallel}^A}{R_{\perp}^{At}} \right] \sigma_n^2 \end{array} \\
 \text{For an arbitrary plane with an angle } \psi = \arctan \frac{\tau_{n1}}{\tau_{nt}} \\
 \left. \begin{array}{l} \text{for } \sigma_n \leq 0 \\ (\tau_{n\psi})^2 = \left(R_{\perp\psi}^A\right)^2 - 2p_{\perp\psi}^c R_{\perp\psi}^A \sigma_n \end{array} \right| \begin{array}{l} \text{for } \sigma_n \geq 0 \\ (\tau_{n\psi})^2 = \left(R_{\perp\psi}^A\right)^2 - 2p_{\perp\psi}^t R_{\perp\psi}^A \sigma_n - \left[ \left(\frac{R_{\perp\psi}^A}{R_{\perp}^{At}}\right)^2 - 2p_{\perp\psi}^t \frac{R_{\perp\psi}^A}{R_{\perp}^{At}} \right] \sigma_n^2 \end{array} \\
 \text{with } \left(\frac{\tau_{n\psi}}{R_{\perp\psi}^A}\right)^2 = \left(\frac{\tau_{nt}}{R_{\perp\perp}^A}\right)^2 + \left(\frac{\tau_{n1}}{R_{\perp\parallel}^A}\right)^2 \text{ and } \frac{p_{\perp\psi}^{t,c}}{R_{\perp\psi}^A} = \frac{p_{\perp\perp}^c}{R_{\perp\perp}^A} \cos^2 \psi + \frac{p_{\perp\parallel}^{t,c}}{R_{\perp\parallel}^A} \sin^2 \psi
 \end{array}$$

**Fig. 6: Analytical relations defining the Puck inter-fibre fracture criteria.**

Starting from the hypotheses of Coulomb and Mohr, now the basis exists for formulating fracture criteria for inter-fibre fracture, using action plane related stresses  $\sigma_n$ ,  $\tau_{nt}$ ,  $\tau_{n1}$  and as anchor points the corresponding fracture resistances  $R_{\perp}^{At}$ ,  $R_{\perp\perp}^A$  and  $R_{\perp\parallel}^A$ . The resulting fracture criteria can be very well visualised by the three-dimensional *Master Fracture Body* in a  $(\sigma_n, \tau_{nt}, \tau_{n1})$ -space (see Fig. 5). According to the fracture hypothesis the areas of the fracture envelope with  $\sigma_n$  compressive stresses and the areas with  $\sigma_n$  tensile stresses on the fracture plane have to be treated individually. For the master fracture body according to Puck, simple functions, i.e. pieces of parabola and ellipse sections, are being used for analytically describing the

longitudinal sections which form the *contour lines* of the master fracture body (see Table in Fig. 6).

When working with action plane related fracture criteria it is typical that the given stresses ( $\sigma_2, \sigma_3, \tau_{23}, \tau_{31}, \tau_{21}$ ) which have been specified in their material ( $x_1, x_2, x_3$ )-coordinate system, have to be transferred into the action-plane related ( $x_1, x_n, x_t$ )-coordinate system. Accordingly, the result of an action-plane related fracture analysis is the  $(\sigma_n^{\text{fr}}, \tau_{nt}^{\text{fr}}, \tau_{n1}^{\text{fr}})$ - stress state at fracture and the corresponding fracture angle  $\theta_{fp}$ . Based on these two results, the fracture stresses can be re-transformed into the lamina coordinate system in order to serve a usual design process. Having calculated numerous individual values of  $(\sigma_2^{\text{fr}}, \sigma_3^{\text{fr}}, \tau_{23}^{\text{fr}}, \tau_{31}^{\text{fr}}, \tau_{21}^{\text{fr}})$ -stresses at fracture, the results can be depicted as a three-dimensional fracture body in the  $(\sigma_{II}, \sigma_{III}, \tau_{\omega 1})$ -stress space [4] (see Fig. 7).

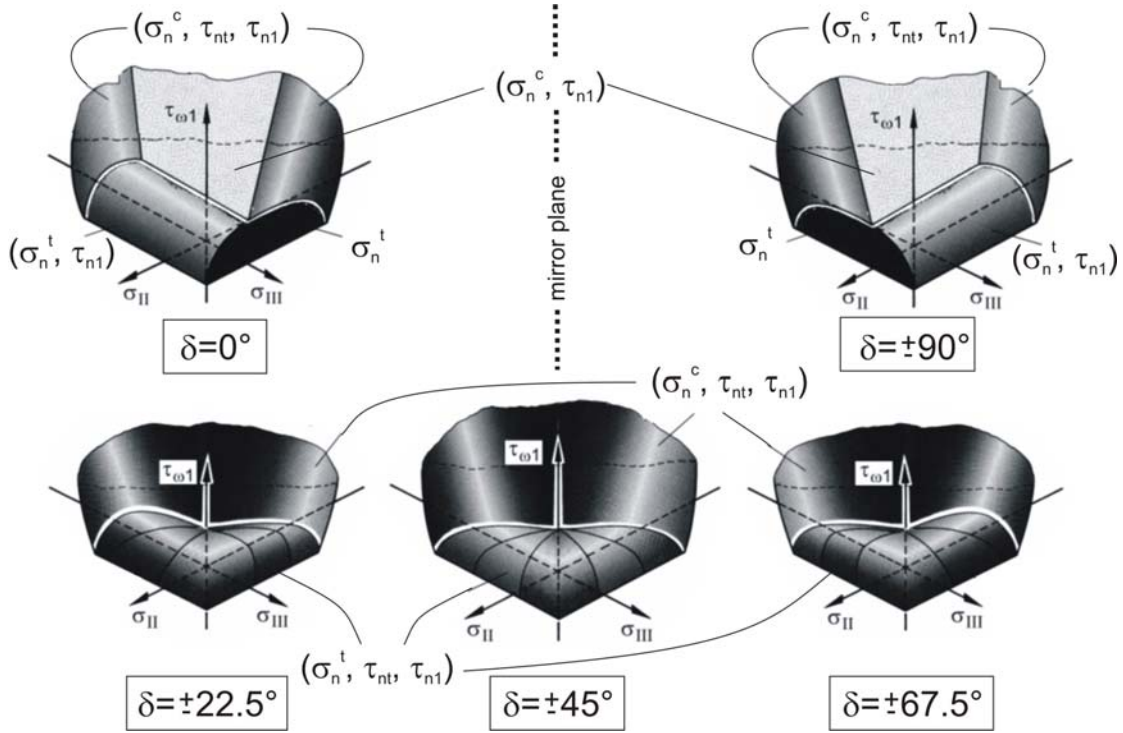


**Fig. 7:**  $(\sigma_{II}, \sigma_{III}, \tau_{\omega 1})$  fracture bodies depending on  $\sigma_{II}, \sigma_{III}$  (principal stresses representing  $\sigma_2, \sigma_3, \tau_{23}$ ) and the parameter  $\delta$  (the angle between the action planes of  $\sigma_{II}$  and  $\tau_{\omega 1}$ , which is the resultant of  $\tau_{21}$  and  $\tau_{31}$ ). The segments of the surface distinguish different fracture modes by different combinations of stresses  $\sigma_n, \tau_{nt}, \tau_{n1}$ .

In order to determine the stresses  $\sigma_n^{\text{fr}}, \tau_{nt}^{\text{fr}}, \tau_{n1}^{\text{fr}}$  at fracture, it is generally necessary to determine the fracture angle by a numerical search first. In the whole space of action planes from  $\theta = -90^\circ$  to  $\theta = +90^\circ$  the stress exposure  $f_E$  has to be calculated

for a reasonable number of inclination angles  $\theta$ . In this way the plane with the highest stress exposure ratio  $f_E$ , that means the potential fracture plane, is found and the corresponding fracture angle  $\theta_{fp}$  is used then to calculate the stresses  $\sigma_n^{fr}$ ,  $\tau_{nt}^{fr}$ ,  $\tau_{n1}^{fr}$  at fracture.  $\theta_{fp}$  is finally used to transform  $(\sigma_n^{fr}, \tau_{nt}^{fr}, \tau_{n1}^{fr})$  into  $(\sigma_2^{fr}, \sigma_3^{fr}, \tau_{23}^{fr}, \tau_{31}^{fr}, \tau_{21}^{fr})$ .

In the course of time, there has been some success in rationalising the cumbersome process of numerical search of the fracture angle and the transformation between the coordinate systems. For some states of stress general analytical solutions have been developed replacing the process described above [16, 17]. In the present paper a contribution has been made to a further rationalisation by developing general analytical solutions for the fracture angles  $\theta_{fp}$  and the fracture stresses not only in the  $(\sigma_n, \tau_{nt}, \tau_{n1})$  stress space but also in the  $(\sigma_2, \sigma_3, \tau_{23})$  stress space, see Sec. 3. This is a good progress for the application but from the didactic point of view an important part of the process – the temporary change of stress space - remains hidden when using analytical solutions.

### 3. Analytical treatment of fractures caused by $(\sigma_2, \sigma_3, \tau_{23})$ -stress combinations

Despite the fact that failure criteria of the Coulomb-Mohr type are three dimensional ab initio, their application has commonly been restricted to in-plane problems. Accordingly the existing publications [15, 16, 17] of the fundamental analytical relations concentrated on  $(\sigma_1, \sigma_2, \tau_{21})$ -stress combinations. Motivated by the excellent performance of the developed numerical implementation of the theory [18, 19, 20], more convenient analytical solutions for  $(\sigma_2, \sigma_3, \tau_{23})$ - load cases have now been derived.

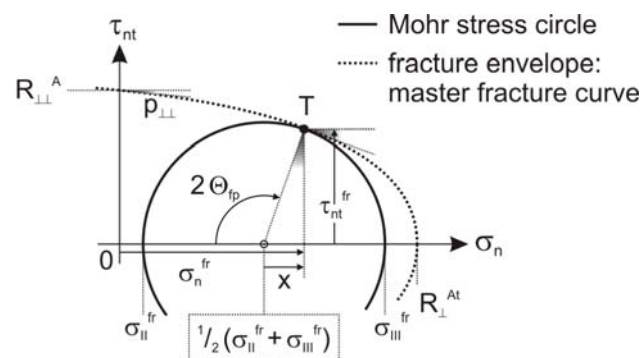


Fig. 8: Mohr's stress circle and fracture curve for a  $(\sigma_2, \sigma_3, \tau_{23})$  load case.

### 3.1 Analytical derivation of fracture curves for $(\sigma_2, \sigma_3, \tau_{23})$ - load cases

At first glance the application of a fracture theory following Coulomb [13] and Mohr [14] appears to be rather straightforward due to the fact, that only three stresses  $(\sigma_n, \tau_{nt}, \tau_{nl})$  and three corresponding fracture resistances of the action plane  $R_{\perp}^{At}, R_{\perp}^A, R_{\parallel}^A$  are involved. However, before fracture stresses can be calculated by an action plane-related fracture criterion, the plane which is closest to fracture has to be identified. Its orientation angle is defined by  $\theta_{fp}$ , which is measured in mathematically positive direction from the thickness direction  $x_3$  to the  $x_t$ -axis tangential to the fracture plane, or in other words from the action plane of  $\sigma_2$  to the action plane of  $\sigma_n$  on the fracture plane. As  $f_{E\ IFF}$  is a measure for the risk of fracture, its highest value is associated with the fracture plane orientation angle  $\theta_{fp}$ .

The basis of the analytical approach is formed by Mohr's and Coulomb's ideas which are combined with Paul's [21] considerations about *intrinsically brittle* materials as well as his modification of the Coulomb/Mohr criterion by introducing *tensile cut-offs*. The considered task is the determination of that plane, which – subjected to increasing load – reaches its fracture condition first. Using the Coulomb/Mohr approach, this mechanical stress to fracture challenge is transferred into a problem of analytical geometry (see Fig. 8). A proportionally increasing  $(\sigma_2, \sigma_3, \tau_{23})$ - stress state is represented by a Mohr stress circle in the  $(\sigma_n, \tau_{nt})$ -diagram, whose diameter grows up to that state of stress where the circle touches the  $(\sigma_n, \tau_{nt})$ -fracture envelope first. As a section through the complete inter-fibre fracture criterion, the master fracture body (MFB, see Fig. 5) [4], this 2D-fracture envelope is referred to as *master fracture curve* in the following. The contact point T between the Mohr stress circle and the  $(\sigma_n, \tau_{nt})$ - master fracture curve denotes both the fracture plane orientation angle  $\Theta_{fp}$  and the fracture stresses  $(\sigma_n^{fr}, \tau_{nt}^{fr})$ . The determination of the contact point T is complicated by the fact that not only the diameter of the circle changes with increasing load but also the position of its centre at  $0.5(\sigma_{II} + \sigma_{III})$ , see Figure 8.

For simplification, the  $(\sigma_2, \sigma_3, \tau_{23})$ -stress state is characterized for the time being by its two principal stresses  $\sigma_{II}$  and  $\sigma_{III}$ , which are, strictly speaking, the external *normal* stresses acting on those two mutually perpendicular fibre-parallel planes that experience no *shear* stress. The parametric representation of the Mohr stress circle is then

$$\sigma_n(\Theta) = \frac{1}{2}(\sigma_{II} + \sigma_{III}) - (\sigma_{III} - \sigma_{II}) \cos(2\Theta) \quad (7)$$

$$\tau_{nt}(\Theta) = \frac{1}{2}(\sigma_{III} - \sigma_{II}) \sin(2\Theta) \quad (8)$$

where every point on this circle belongs to a fibre-parallel plane in the UD lamina, inclined by the angle  $\Theta$ . It is very important to realise that in Eqs. 7 and 8 the orientation of the fracture plane is not given by the angle  $\theta_{fp}$  which defines the inclination of the action plane against the action plane of an applied  $\sigma_2$ . Eqs. 7 and 8 are defined in principal stresses instead, accordingly the orientation  $\Theta_{fp}$  is measured between the action plane of the principal stress  $\sigma_{II}$  and the fracture plane.

The master fracture curve, up to which the circle may grow while moving its centre, is defined as a parabola in the  $\sigma_n \leq 0$ -domain [4]:

$$\left(\tau_{nt}^{fr}\right)^2 = \left(R_{\perp\perp}^A\right)^2 - 2p_{\perp\perp} R_{\perp\perp}^A \sigma_n^{fr} \quad (9)$$

In the case of  $\sigma_n \geq 0$ , the master fracture curve is chosen as an ellipse:

$$\left(\tau_{nt}^{fr}\right)^2 = \left(R_{\perp\perp}^A\right)^2 - C_1 \sigma_n^{fr} - C_2 \left(\sigma_n^{fr}\right)^2 \quad (10)$$

where  $C_1 = 2p_{\perp\perp} R_{\perp\perp}^A$  and  $C_2 = \left(\frac{R_{\perp\perp}^A}{R_{\perp\perp}^{At}}\right)^2 - 2p_{\perp\perp} \frac{R_{\perp\perp}^A}{R_{\perp\perp}^{At}}$

For the coordinates  $(\sigma_n^{fr}, \tau_{nt}^{fr})$  of the contact point  $T$ , both the equations of the Mohr stress circle, Eqs. 7 and 8, and the equation of the master fracture curve (Eq. 9 or Eq. 10, respectively) are satisfied and the gradients of the Mohr stress circle and the fracture envelope are identical. The mathematical expressions of these two conditions lead to an analytical relation between:

- the master fracture curve in the  $(\sigma_n, \tau_{nt})$ -stress space where the fracture criterion is originally defined, and
- the fracture curve in a  $(\sigma_{II}, \sigma_{III})$ -stress space which represents the sustainable externally applied stresses  $(\sigma_2^{fr}, \sigma_3^{fr}, \tau_{23}^{fr})$ .

In Figure 8, the two basic geometric relations for the derivation are visualized:

$$\begin{aligned} \sigma_n^{fr} &= \frac{1}{2}(\sigma_{II}^{fr} + \sigma_{III}^{fr}) + x \\ x &= -\left(\frac{d\tau_{nt}}{d\sigma_n}\right)_T \tau_{nt}^{fr} \end{aligned} \quad (11)$$

For  $\sigma_n \leq 0$ , the implicit differentiation of the parabola Eq. 13 leads to

$$2\tau_{nt}^{fr} \left(\frac{d\tau_{nt}}{d\sigma_n}\right)_T = -2p_{\perp\perp} R_{\perp\perp}^A \quad (12)$$

With Eq. 11 we derive

$$x = p_{\perp\perp} R_{\perp\perp}^A \quad (13)$$

and we get for  $\sigma_n^{fr}$  at fracture

$$\sigma_n^{fr} = \frac{1}{2}(\sigma_{II}^{fr} + \sigma_{III}^{fr}) + p_{\perp\perp} R_{\perp\perp}^A \quad (14)$$

Together with Eq. 7 the fracture plane orientation angle  $\Theta_{fp}$  can be calculated from

$$\cos(2\Theta_{fp}) = \frac{-2p_{\perp\perp} R_{\perp\perp}^A}{(\sigma_{III}^{fr} - \sigma_{II}^{fr})} \quad (15)$$

Keeping in mind the aim of transferring the parabola part of the master fracture curve into the  $(\sigma_{II}, \sigma_{III})$ -stress space, the  $(\tau_{nt}^{fr})^2$  in the parabola Eq. 9 may be replaced by the squared Eq. 8 which introduces a  $\Theta$ -dependency. Knowing that  $\sin^2(2\Theta) = 1 - \cos^2(2\Theta)$ , the relation of Eq. 15 substitutes  $\Theta$  and the  $\sigma_n$  in the parabola Eq. 9 may be replaced by Eq. 14.

The arising relation is the parabola part of the master fracture curve transferred into the  $(\sigma_{II}^{fr}, \sigma_{III}^{fr})$ -stress space:

$$\frac{1}{4}(\sigma_{III}^{fr} - \sigma_{II}^{fr})^2 = (R_{\perp\perp}^A)^2 \left[ 1 - (p_{\perp\perp})^2 \right] - p_{\perp\perp} R_{\perp\perp}^A (\sigma_{III}^{fr} + \sigma_{II}^{fr}) \quad (16)$$

It describes a parabola which is symmetric with respect to the  $(\sigma_{II}^{fr} + \sigma_{III}^{fr})$ -axis.

For  $\sigma_n \geq 0$ , the ellipse part of the master fracture curve is transferred into the  $(\sigma_{II}, \sigma_{III})$ -stress space by the same procedure as that used for the parabola part leading to an equation of an ellipse in the  $(\sigma_{II}, \sigma_{III})$ -space which is also symmetric with respect to the  $(\sigma_{II}^{fr} + \sigma_{III}^{fr})$ -axis:

$$\frac{1}{4}(\sigma_{III}^{fr} - \sigma_{II}^{fr})^2 = (R_{\perp\perp}^A)^2 \left[ 1 - \frac{(p_{\perp\perp})^2}{1 - C_2} \right] - \frac{p_{\perp\perp} R_{\perp\perp}^A}{1 - C_2} (\sigma_{III}^{fr} + \sigma_{II}^{fr}) - \frac{C_2}{4(1 - C_2)} (\sigma_{III}^{fr} + \sigma_{II}^{fr})^2 \quad (17)$$

It can be shown that for the whole region of validity of Eq. 17 the nominator will satisfy the following condition:  $1 - C_2 \geq 0$ . The analytical solutions for  $x$ ,  $\sigma_n^{fr}$  and  $\Theta_{fp}$  are

$$x = p_{\perp\perp} R_{\perp\perp}^A + C_2 \sigma_n^{fr} \quad (18)$$

$$\sigma_n^{fr} = \frac{0.5(\sigma_{III}^{fr} + \sigma_{II}^{fr}) + p_{\perp\perp} R_{\perp\perp}^A}{1 - C_2} \quad (19)$$

$$\cos(2\Theta_{fp}) = -\frac{C_2 (\sigma_{III}^{fr} + \sigma_{II}^{fr}) + 2p_{\perp\perp} R_{\perp\perp}^A}{(1 - C_2) (\sigma_{III}^{fr} - \sigma_{II}^{fr})} \quad (20)$$

For a complete definition of the IFF fracture curve in the  $(\sigma_{II}, \sigma_{III})$ - stress space, we have to define where, in the  $(\sigma_{II}, \sigma_{III})$ -stress space, the parabolic part and where the elliptical part forms the valid fracture curve.

Eq. 14 and Eq. 19 show the dependency of  $\sigma_n^{fr}$  on  $\sigma_{II}^{fr}$  and  $\sigma_{III}^{fr}$ . Seeing that in the first quadrant, both stresses  $\sigma_{II}^{fr}$  and  $\sigma_{III}^{fr}$  are positive,  $\sigma_n^{fr}$  is also positive and not zero. In the third quadrant, both stresses are negative and therefore, according to Eq. 14,  $\sigma_n^{fr}$  is also negative and not zero. From that finding it can be concluded that the situation  $\sigma_n^{fr} = 0$  does only exist in the second and fourth quadrants, where  $\sigma_{II}^{fr}$  and  $\sigma_{III}^{fr}$  have different signs. Putting  $\sigma_n^{fr} = 0$  into Eq. 14 results in

$$(\sigma_{III}^{fr} + \sigma_{II}^{fr}) = -2p_{\perp\perp} R_{\perp\perp}^A \quad (21)$$

Putting this into Eq. 16 results in

$$(\sigma_{III}^{fr} - \sigma_{II}^{fr}) = \pm 2 R_{\perp\perp}^A \sqrt{1 + (p_{\perp\perp})^2} \quad (22)$$

From these two equations, valid for  $\sigma_n^{fr} = 0$ , it can be concluded that for the border line between  $\sigma_n^{fr} < 0$  and  $\sigma_n^{fr} > 0$  the following relationship exists (see Fig. 9):

$$\frac{\sigma_{III}^{fr} + \sigma_{II}^{fr}}{\sigma_{III}^{fr} - \sigma_{II}^{fr}} = \pm \frac{p_{\perp\perp}}{\sqrt{1 + (p_{\perp\perp})^2}} \quad (23)$$

This means that in the third and fourth quadrants the parabolic fracture curve, Eq. 16 for  $\sigma_n^{fr} \leq 0$  is the valid one as long as

$$\left| \frac{\sigma_{III} + \sigma_{II}}{\sigma_{III} - \sigma_{II}} \right| \geq \left| \frac{p_{\perp\perp}}{\sqrt{1 + (p_{\perp\perp})^2}} \right| \quad (24)$$

If the condition according to Eq. 24 is not fulfilled the elliptical fracture curve Eq. 17 is valid in the 2<sup>nd</sup> or 4<sup>th</sup> quadrant, see Figure 6. There is a further limitation of the

validity of the developed  $(\sigma_{II}, \sigma_{III})$ -fracture conditions. Neither the stress  $\sigma_{II}$  nor the stress  $\sigma_{III}$  will ever be able to exceed  $R_{\perp}^{At}$  (see Fig. 9).

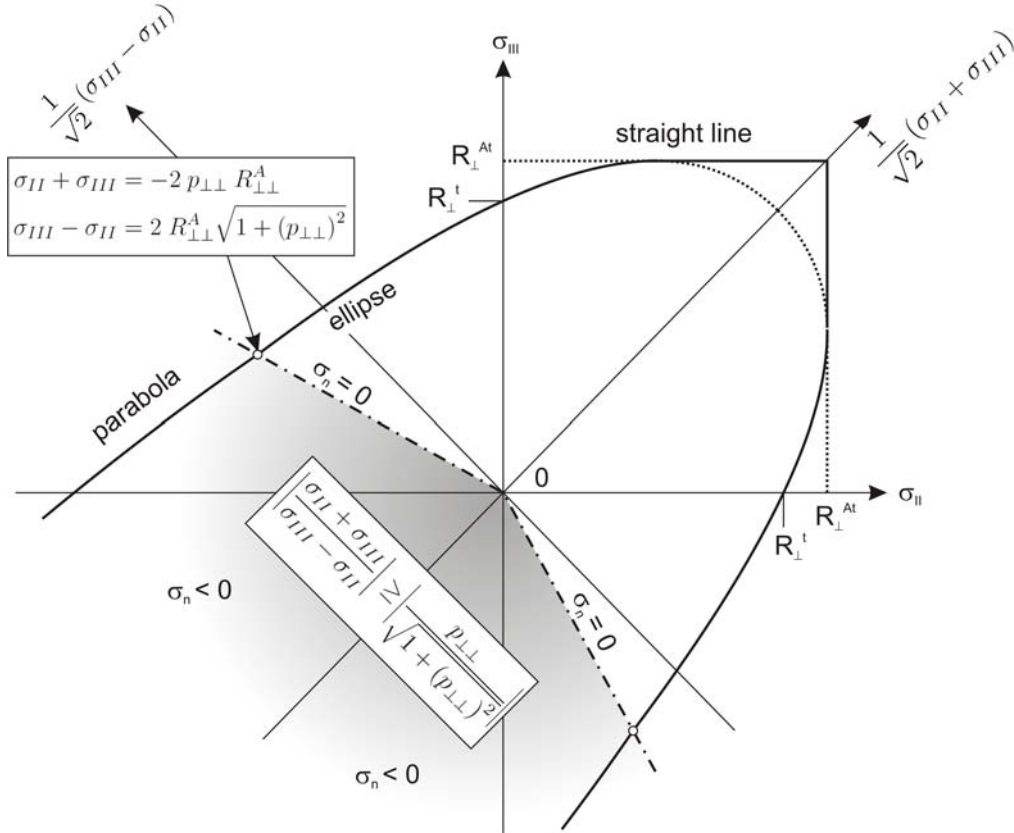


**Fig. 9: Characterisation of the limits of validity of the parabolic, the elliptical and the straight fracture envelopes for a UD-composite subjected to a  $(\sigma_2, \sigma_3, \tau_{23})$ -state of stress, the principal stresses of which are  $\sigma_{II}$  and  $\sigma_{III}$ .**

If one or both of the two stresses reach this limit before the Mohr stress circle touches the Master fracture curve on any other point, the material fractures due to pure tensile  $\sigma_n$  on the fracture plane with the fracture angle  $\Theta_{fp} = 0^\circ$  or  $\Theta_{fp} = 90^\circ$ . In the  $(\sigma_{II}, \sigma_{III})$ -stress space these states of fracture are represented by two straight lines:

$$\sigma_{II}^{fr} = R_{\perp}^{At} \text{ and } \sigma_{III}^{fr} = R_{\perp}^{At} \quad (25)$$

If the straight lines hit the  $(\sigma_{II}^{fr}, \sigma_{III}^{fr})$  fracture curve where the parabolic part is valid (for  $\sigma_n \leq 0$ ), they are called *tensile cut-offs* and the associated material behaviour is called *intrinsically brittle* [21].

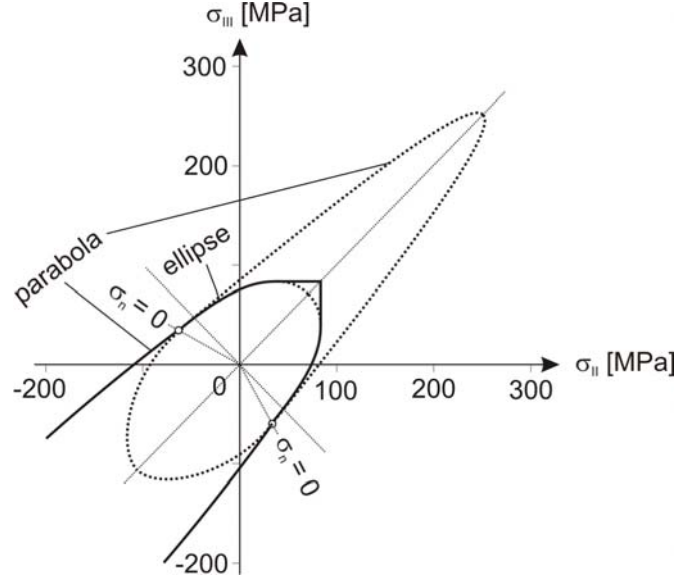


**Fig.10: Total view of the shape of the three different  $(\sigma_{II}, \sigma_{III})$ -fracture curves (calculated with material properties of WWFE-II Test Case 1 [19]).**

Let's now have a closer look at the straight lines in Eq. 25 and the elliptical  $(\sigma_{II}^{fr}, \sigma_{III}^{fr})$ -fracture curve according to Eq. 17. At first sight one could expect a similar tensile cut-off as it is known for the parabolic  $(\sigma_{II}^{fr}, \sigma_{III}^{fr})$ -fracture curves. But this is not true, the straight line  $\sigma_{III}^{fr} = R_{\perp}^{At}$  for instance touches the ellipse only in one point, namely the point in which the ellipse shows its maximum  $\sigma_{III}^{fr}$  value. This can be concluded from the fact that the quadratic equation by which intersections of straight line and ellipse can be detected does not show two solutions but only one. Normally, a quadratic equation has two solutions because the solution consists of the sum of a linear form and a  $\pm$ square root. But in the case in question the root term is zero. The contact point of the straight line  $\sigma_{III}^{fr} = R_{\perp}^{At}$  has a  $\sigma_{II}^{fr}$  coordinate which can be calculated from

$$\sigma_{II}^{fr} = (1 - C_2)R_{\perp}^{At} - 2p_{\perp\perp} R_{\perp\perp}^A \quad (26)$$

with  $C_2$  from Eq. 10

This smooth transition from the fracture mode of the combined  $\tau_{\perp\perp}$ - and  $\sigma_{\perp}^t$ -stressing (on the ellipse) to a pure  $\sigma_{\perp}^t$ -fracture mode on the straight line  $\sigma_{III}^{fr} = R_{\perp}^{At}$  or  $\sigma_{II}^{fr} = R_{\perp}^{At}$  is illustrated in Figures 9 to 12.

In Figs. 9, 10, 11, 12c and 14, it can be seen that if the fracture mode transition is taken into consideration the upper part of the ellipse is covered by a rather small cap with a rectangular corner. That means that in this region, "strength" is being added to that one shown by the elliptical fracture envelope. This is a quite different situation compared to that one in the region of  $\sigma_n \leq 0$  where the parabolic fracture is valid. There the fracture mode transition cuts off parts of the parabolic fracture curve, see

Figure 9a, and the “strength” is diminished. There the expression “tensile cut-off” is correct. This is not the same for the elliptical fracture curve.

The sharp 90° corners of the fracture envelope predicted by the transition to the pure tensile fracture mode are unrealistic for probabilistic reasons. The use of numerical search of the fracture angle allows a physically reasonable “rounding” to be achieved by the  $\eta_{m+p}$  weakening procedure [4]. However, if the analytical solutions for the fracture stresses are used then one should seek to obtain another suitable rounding technique. In both cases, if the ‘cap’ on the ellipse is very small, it is perhaps reasonable to neglect it completely and rely on the elliptic fracture curve as being the valid one throughout. In this case one can expect to stay conservative.

### 3.2 Analytical relations for the stress exposure ratio

Up to this point it has been dealt with the  $(\sigma_{II}^{fr}, \sigma_{III}^{fr})$ -fracture curves focussing on the question whether the applied stresses are bearable or not. In this paragraph the results are presented in different form, which is especially suited for engineering application. During the design process, the question is not only whether or not a given stress state leads to fracture but also how far a given stress state is away from fracture. Assuming that all the applied stresses increase *proportionally* up to the fracture, the inter-fibre stress exposure  $f_{EIFF}$  is the relevant measure which linearly grows from 0 to the fracture condition  $f_{EIFF} = 1$ . The reciprocal, the stretch factor,  $f_{SIFF} = 1/f_{EIFF}$  is regarded as a measure of a safety factor [4]. Because the fracture conditions (Eqs. 16 and 17) are functions of the first and second order in the stresses the stress exposure  $f_E$  can be calculated according to Eq. 12 in [4]. From Eq. 16 the IFF stress exposure for  $\sigma_n \leq 0$  and the acting stresses  $\sigma_{II}$  and  $\sigma_{III}$  is

$$f_{EIFF} = \frac{p_{\perp\perp} \left( \sigma_{III} + \sigma_{II} \right) + \sqrt{\left[ p_{\perp\perp} \left( \sigma_{III} + \sigma_{II} \right) \right]^2 + \left[ 1 - \left( p_{\perp\perp} \right)^2 \right] \left( \sigma_{II} - \sigma_{III} \right)^2}}{2 \left[ 1 - \left( p_{\perp\perp} \right)^2 \right] R_{\perp\perp}^A} \quad (27)$$

and for  $\sigma_n \geq 0$  from Eq. 17

$$f_{EIFF} = \frac{1}{K} \left\{ C_1 \left( \sigma_{III} + \sigma_{II} \right) + \sqrt{\left[ C_1 \left( \sigma_{III} + \sigma_{II} \right) \right]^2 + K \left[ \left( \sigma_{III} - \sigma_{II} \right)^2 + 4C_2 \sigma_{II} \sigma_{III} \right]} \right\}$$

$$\text{with } K = 4 \left( R_{\perp\perp}^A \right)^2 \left[ 1 - C_2 - \left( p_{\perp\perp} \right)^2 \right] \quad (28)$$

For cases in which the straight line envelope, Eq. 25, is valid, the IFF stress exposure is simply

$$f_E = \frac{\sigma_{II,III}}{R_{\perp}^{At}} \quad (29)$$

### 3.3 Discussion of the $(\sigma_{II}, \sigma_{III})$ -fracture curves

#### 3.3.1 Symmetry and Invariance

The parabolic and the elliptical part of the  $(\sigma_{II}, \sigma_{III})$  fracture curve meet each other on two points on the boundary line for which  $\sigma_n = 0$ . This line has a small kink at the origin of the coordinate system (see Fig. 9 and 10). In their point of contact parabola and ellipse have the same gradient that means the two curves join without any discontinuity. However, this requires the inclination parameters  $p_{\perp}^c$  and  $p_{\perp}^t$  to be the same. In previous publications on Puck's fracture criteria a choice was given to the use of different values for  $p_{\perp}^c$  and  $p_{\perp}^t$  but equal values were advised. In the meantime, experience has shown that there is really no need for different  $p_{\perp}^c$  and  $p_{\perp}^t$ , in the contrary,  $p_{\perp}^c \neq p_{\perp}^t$  leads to a undesired discontinuity in the  $(\sigma_{II}, \sigma_{III})$ -fracture curve, see above. Therefore, we now strongly recommend to use  $p_{\perp}^c = p_{\perp}^t = p_{\perp}$  [19].

The  $(\sigma_{II}, \sigma_{III})$ -fracture curve, composed of a parabolic section for  $\sigma_n \leq 0$  (according to Eq. 16) and an elliptical section valid for  $\sigma_n \geq 0$  (according to Eq. 17), is symmetric with respect to the line  $\sigma_{II} = \sigma_{III}$ . The latter axis also corresponds to the diagonal  $\frac{1}{\sqrt{2}}(\sigma_{III} + \sigma_{II})$ -axis. This implies that the central axis of the  $(\sigma_{II}, \sigma_{III})$ -fracture curve is rotated just  $+45^\circ$  or  $-45^\circ$  with respect to the  $\sigma_{II}$ -axis or the  $\sigma_{III}$ -axis, respectively. Bearing in mind that the stresses  $\sigma_{II}$  and  $\sigma_{III}$  are both transverse stresses, they are therefore equivalent and the designation used for  $\sigma_{II}$  and  $\sigma_{III}$  is arbitrary. Consequently, the  $\sigma_{II}$ -axis and the  $\sigma_{III}$ -axis are interchangeable.

So far, we have written the fracture conditions with the variables  $\sigma_{II}$  and  $\sigma_{III}$  and have avoided the use of  $\sigma_2, \sigma_3, \tau_{23}$ . That was necessary because we wanted to make use of the rather simple geometries approach which is made possible by the Eqs. (7) and (8) for Mohr's circle. But it is no problem now to rewrite the fracture conditions using the values  $\sigma_2, \sigma_3, \tau_{23}$  which are normally used to present the given stresses. For transversely isotropic material, it does not matter if the stresses are given in the  $(x_{II}, x_{III})$ -coordinate system or in the  $(x_2, x_3)$ -coordinate system. Any arbitrary coordinate system can be used without changing the results of a fracture analysis. In other words the fracture conditions must be invariant against a rotation of the coordinate system around the  $x_1$ -axis, while the stress combination is unchanged.

In Eq. 20 and Eq. 21 only the sum  $(\sigma_{II} + \sigma_{III})$  and the difference  $(\sigma_{II} - \sigma_{III})$  appear as variables. Both are invariants and could be re-placed using  $\sigma_{II} + \sigma_{III} = \sigma_2 + \sigma_3$ :

$$\frac{1}{4}(\sigma_{II} - \sigma_{III})^2 = \frac{1}{4}(\sigma_2 - \sigma_3)^2 + \tau_{23}^2 \quad (30)$$

The product  $\sigma_{II} \cdot \sigma_{III}$  which is appearing in Eq. 28 can be replaced in the following way:

$$\sigma_{II} \sigma_{III} = \sigma_2 \sigma_3 - \tau_{23}^2 \quad (31)$$

If the  $(\sigma_{II}, \sigma_{III})$ -fracture conditions are rewritten with those invariant they can be used for given  $\sigma_2, \sigma_3, \tau_{23}$  values without first calculating the principal stresses  $\sigma_{II}$  and  $\sigma_{III}$ .

### 3.3.2 Fracture angles

In the following paragraph some interesting observations of the fracture angles  $\Theta_{fp}$  at certain places of the  $(\sigma_{II}, \sigma_{III})$ -fracture curve are discussed. Figure 11 shows the total  $(\sigma_{II}, \sigma_{III})$ - fracture curve for a material with a rather high action plane fracture resistance  $R_{\perp}^{At}$ . On every line which is parallel to the axis where  $\sigma_{III} = -\sigma_{II}$  we find fracture angles  $\Theta_{fp}$  which differ from  $\pm 45^\circ$  by the same small angle, designated by the symbol  $\lambda$ . For the upper curve (valid for  $\sigma_{II} < \sigma_{III}$ ) the fracture angle is  $\Theta_{fp} = \pm(45^\circ + \lambda)$  and for the lower curve (valid for  $\sigma_{II} > \sigma_{III}$ ) the corresponding fracture angle is  $\Theta_{fp} = \pm(45^\circ - \lambda)$ . At the point belonging to uniaxial compression we get from Eq. 19 with the material data for Test Case 1 of the WWFE-II [11, 19] a fracture angle of  $\Theta_{fp} = \pm(45^\circ + 2.7^\circ) = \pm 47.7^\circ$  on the upper curve and  $\Theta_{fp} = \pm(45^\circ - 2.7^\circ) = \pm 42.3^\circ$  on the lower curve. There are rather little differences of the angle  $\Theta_{fp}$  in the area where  $\sigma_n \leq 0$  but a more rapid change of  $\Theta_{fp}$  takes place in the area where  $\sigma_n \geq 0$ . On the straight line envelopes the fracture angle is of course  $90^\circ$  or  $0^\circ$ . In Figure 11a and 11b, it is demonstrated how also in Mohr's circles for the upper and lower part of the  $(\sigma_{II}, \sigma_{III})$ -fracture curve the difference in fracture angle ( $|\Theta_{fp}| = 45^\circ + \lambda$  or  $|\Theta_{fp}| = 45^\circ - \lambda$ ) can be seen.

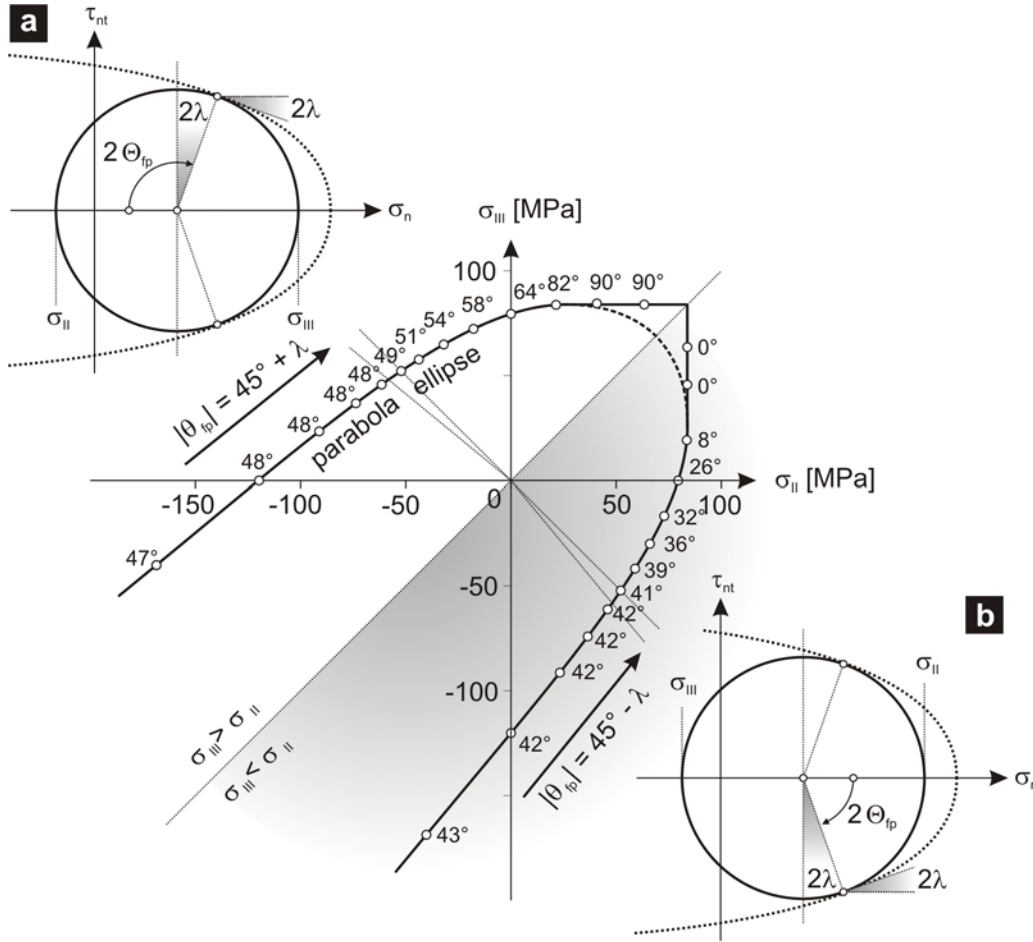
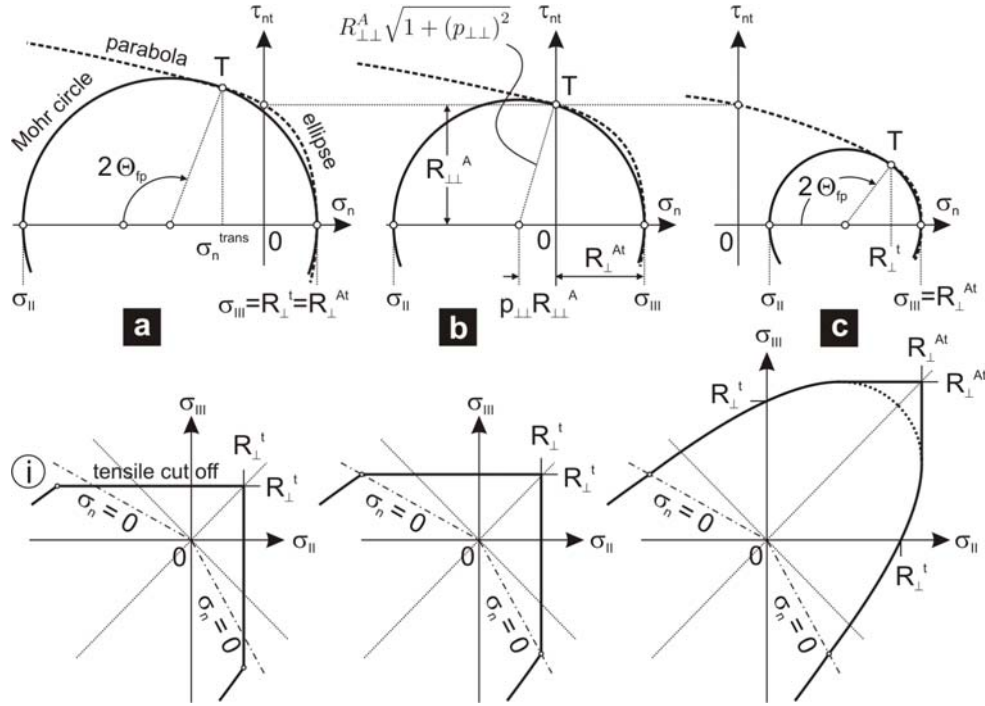


Fig. 11: Appearing fracture angles  $\Theta_{fp}$  [°] in Test Case 1 of the WWFE-II and associated Mohr's circles. (a) for  $\sigma_{II} < \sigma_{III}$ , (b) for  $\sigma_{II} > \sigma_{III}$ .

## 4 Intrinsically and non-intrinsically brittle behaviour

### 4.1 Material behaviour

The phenomena which will be discussed in this chapter are illustrated in details in Figure 12. Within every master fracture curve a Mohr stress circle can be drawn which touches the master fracture curve at  $T = (\sigma_n^{fr,trans}, \tau_{nt}^{fr} \neq 0)$  and at  $(\sigma_n^{fr} = R_{\perp}^{At}, \tau_{nt}^{fr} = 0)$  at the same time. This circle is called *transition circle* (see Fig12, upper row). It represents the limit between two domains of load cases, namely those which lead to fractures with combined  $(\sigma_n^{fr}, \tau_{nt}^{fr})$  on the fracture plane and those which lead to fractures due to pure tensile  $\sigma_n$ . For geometrical reasons,  $\sigma_n^{fr,trans}$  is the maximum  $\sigma_n$  value for which combined  $(\sigma_n^{fr}, \tau_{nt}^{fr})$ -fractures occur before the fractures shift to pure tensile fractures. The  $(\sigma_{II}, \sigma_{III})$  stress state, which characterizes the transition circle is that point in the  $(\sigma_{II}, \sigma_{III})$ -stress space, where the straight line envelope meets the  $(\sigma_{II}, \sigma_{III})$ -fracture curve (see Fig. 12, i).



**Fig. 12: Illustrations of intrinsically and non-intrinsically brittle behaviour: (a) intrinsically brittle, (b) at the limit of intrinsically brittle and (c) non-intrinsically brittle.**

The value of  $\sigma_n^{trans}$  is a central parameter defining whether a material behaves *intrinsically brittle* [21] or not. By definition, an intrinsically brittle material will never break due to a combined  $(\sigma_n^{tensile}, \tau_{nt})$  stress state on its fracture plane, hence there is  $\sigma_n^{trans} \leq 0$  for these materials. As a consequence, the contact point T will always be found on the parabolic part of the master fracture curve. An elliptical part of the master fracture curve, which would be valid in a  $\sigma_n^{trans} \geq 0$  domain does not exist for an intrinsically brittle material. The only material properties which are involved in the fracture process where the parabolic fracture curve is the valid one are  $R_{\perp\perp}^A$  and  $p_{\perp\perp}$ .

The shape of the master fracture curve for *non-intrinsically brittle* material behaviour allows  $\sigma_n^{fr,trans} \geq 0$  and thus fractures with combined  $(\sigma_n^{fr,tensile}, \tau_{nt}^{fr})$ -stress state on the fracture plane. According to that with non-intrinsically brittle material the shape of an elliptical part of a master fracture curve does influence the fracture process. In the  $(\sigma_{II}, \sigma_{III})$ -fracture condition now in addition to  $R_{\perp\perp}^A$  and  $p_{\perp\perp}$  also  $R_{\perp}^{At}$  appears (see Eq. 17 and 10).

The difference between both material behaviours becomes most obvious by studying a uniaxial transverse tensile case. An increasingly applied tensile  $\sigma_2$  or  $\sigma_3$  (which equals a pure  $\sigma_{II}$  or  $\sigma_{III}$  stress in terms of principal stresses) is represented by a growing Mohr stress circle which eventually touches the master fracture curve. In case of an *intrinsically brittle* material behaviour the Mohr stress circle first touches

the master fracture curve at  $T(\sigma_n^{fr} = \sigma_{III} = R_{\perp}^{At}, \tau_{nt}^{fr} = 0)$ , see Fig. 12a. The physical meaning is, that such a material breaks due to an applied uniaxial tension in the very action plane of the applied tension and therefore the fracture resistance of the action plane  $R_{\perp}^{At}$  equals the experimentally determined uniaxial transverse tensile strength  $R_{\perp}^t$ .

In contrast to that, a non-intrinsically brittle material may fail due to a combined  $(\sigma_n^{fr,trans}, \tau_{nt}^{fr})$  stress state on an inclined fracture plane. In such a case  $R_{\perp}^{At}$  is *not identical* with the uniaxial transverse tensile strength  $R_{\perp}^t$  of the material. The fracture resistance  $R_{\perp}^{At}$  has either to be determined by the parameter identification approach below (see Sec. 4.2) or to be measured experimentally by a  $\sigma_{II} = \sigma_{III}$  load case. In such a load case, no  $\tau_{nt} = \frac{1}{2}(\sigma_{III} - \sigma_{II}) \sin(2\Theta)$  is acting on any action plane (see Fig. 11), and thus the fracture will occur due to pure tensile  $\sigma_n^{fr} = \sigma_{II}^{fr} = \sigma_{III}^{fr} = R_{\perp}^{At}$  on an arbitrary plane.

The constellation of the material parameters  $(R_{\perp\perp}^A, R_{\perp}^{At}, p_{\perp\perp})$  involved in the Eqs. 9 and 10 defines the shape of the master fracture curve and thus the basic fracture behaviour of a material mentioned above. It can be shown in the upper part of Figure 12b, that the radius,  $r_M$ , of the shown Mohr circle for the material, which is just at the limit of intrinsically brittle behaviour can be expressed in two different ways

$$r_M = R_{\perp\perp}^A \sqrt{1 + (p_{\perp\perp})^2} = p_{\perp\perp} R_{\perp\perp}^A + R_{\perp}^{At} \quad (32)$$

Re-arrangement leads to the following formula for the limit of intrinsically brittle behaviour:

$$\frac{1}{2} \left( \frac{R_{\perp\perp}^A}{R_{\perp}^{At}} - \frac{R_{\perp}^{At}}{R_{\perp\perp}^A} \right) > p_{\perp\perp} \quad (33)$$

This means that there is intrinsically brittle behaviour as long as Eq. 33 is valid.

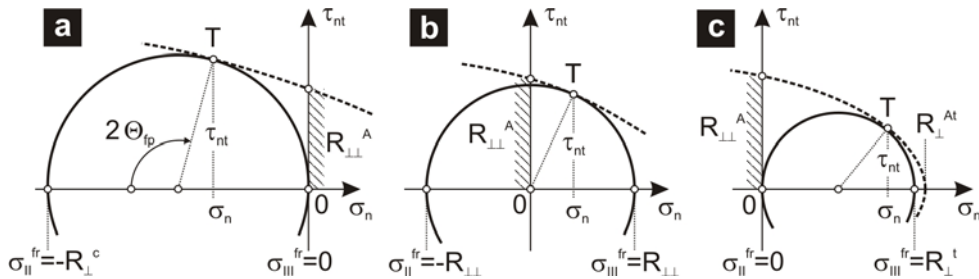


**Fig. 13: Mohr circles and master fracture curve (a) for uniaxial transverse compression, (b) for pure transverse/transverse shear and (c) for uniaxial transverse tension. All stresses at their fracture limit.**

From the experimental point of view, intrinsically brittle behaviour can also be identified by looking at the transverse tensile strength  $R_{\perp}^t$  and the transverse/transverse shear strength  $R_{\perp\perp}$ . In the  $(\sigma_n, \tau_{nt})$ -diagram the former load case is characterised by  $(\sigma_{II}=0, \sigma_{III})$ , see figure 13c, the latter one by  $(\sigma_{II}=-\sigma_{III})$ , see Figure 13b. For an intrinsically brittle material, both Mohr stress circles for both cases meet the master fracture curve on the  $\sigma_n$ -axis where  $\sigma_n = \sigma_{III} = R_{\perp}^{At}$ . As the bearable amount of applied  $\tau_{23}$  equals  $|\sigma_{II}| = |\sigma_{III}|$  in the transverse/transverse shear load case, there is

$$R_{\perp\perp} = R_{\perp}^t = R_{\perp}^{At} \quad (34)$$

for an intrinsically brittle material.

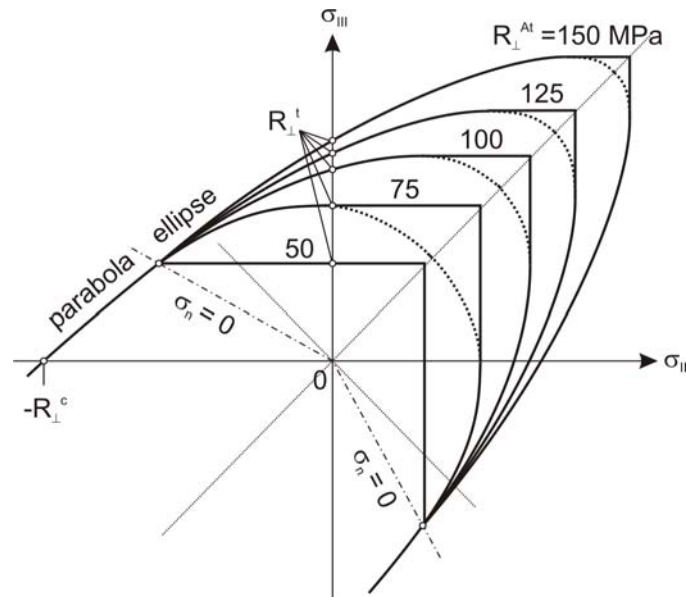


**Fig. 14:  $(\sigma_{II}, \sigma_{III})$  fracture curves calculated with  $R_{\perp\perp}^A = 64\text{MPa}$ ,  $p_{\perp\perp} = 0.25$  and different  $R_{\perp}^{At}$ .**

Up to now, in former applications of the Puck theory slight differences between experimental  $R_{\perp\perp}$  and  $R_{\perp}^t$  values have been neglected and all the common UD fibre reinforced polymers were treated as intrinsically brittle material. Reported differences between these two strengths have been attributed to experimental inaccuracies as the experimental determination of  $R_{\perp\perp}$  is extremely difficult. Accordingly, the fracture resistance of the action plane  $R_{\perp}^{At}$  has been set equal to the experimentally determined  $R_{\perp}^t$  and the transverse/transverse shear strength  $R_{\perp\perp}$  has not been used for the parameter definition of the inter-fibre criterion. Thus the measured  $R_{\perp\perp}$  has not been exactly met by the fracture prediction. The authors now expect some common UD fibre reinforced polymer composites to be just in the transition zone between intrinsically brittle and non-intrinsically brittle behaviour. Figure 14 demonstrates the

dependence of the  $(\sigma_{II}, \sigma_{III})$ -fracture curve of non-intrinsically brittle material from the magnitude of the tensile fracture resistance  $R_{\perp}^{At}$ .

#### 4.1 Parameter identification: Fracture resistances of the action plane $R^A$

This section presents a new approach for the determination of IFF parameters in the case of *non*-intrinsically brittle behaviour. The  $(\sigma_n, \tau_{nt}, \tau_{n1})$ -master fracture body is calibrated by the three action plane resistances  $R_{\perp}^{At}$ ,  $R_{\perp\perp}^A$ ,  $R_{\perp\parallel}^A$  only. They represent the distances from the origin of the coordinate system to the points where the  $\sigma_n$ -,  $\tau_{nt}$ -,  $\tau_{n1}$ - stress axes intersect the fracture envelope. The shape of the master fracture body is fixed by the decision that the contour lines which form the rim of longitudinal sections through the master fracture body should be parabolic where  $\sigma_n \leq 0$  and elliptical where  $\sigma_n \geq 0$ . Their gradients in the anchor point are given by  $p_{\perp\perp}$ ,  $p_{\perp\parallel}^c$ ,  $p_{\perp\parallel}^t$  which can be varied to a certain degree, normally 0.1 to 0.3 (see Table 1 in [4]). Please remember that we definitely have given up to distinguish  $p_{\perp\perp}^c$ ,  $p_{\perp\perp}^t$  and are now using  $p_{\perp\perp}$  only.

Section 4 did not deal with transverse/parallel shear stressing  $\tau_{\perp\parallel}$  and the associated action plane resistance  $R_{\perp\parallel}^A$  has not been mentioned. For  $\tau_{\perp\parallel}$ -shear stressing there is no doubt that always

$$R_{\perp\parallel}^A = R_{\perp\parallel} \quad (35)$$

is valid. This is due to the fact that under  $\tau_{\perp\parallel}$ -shear stressing the plane of the application of  $\tau_{\perp\parallel}$  is also the plane with the highest stress exposure  $f_E$  and therefore also the fracture plane.

As already mentioned a comparable situation exists for  $R_{\perp}^{At}$  if the material behaves intrinsically brittle. In this case  $R_{\perp}^t$  is identical with the usual transverse tensile strength given as follows:

$$R_{\perp}^{At} = R_{\perp}^t \quad (36)$$

For intrinsically brittle and non-intrinsically brittle material  $R_{\perp\perp}^A$  can not be determined by a simple test. Up to now  $R_{\perp\perp}^A$  has been derived from the result of a

uniaxial transverse compression test. If  $\sigma_{II} = -R_{\perp}^c$  and  $\sigma_{III} = 0$  (see Figure 13a) are inserted into Eq. 16 the following relationship is found

$$R_{\perp\perp}^A = \frac{R_{\perp}^c}{2(1 + p_{\perp\perp})} \quad (37)$$

For the still unknown parameters  $R_{\perp}^{At}$  and  $p_{\perp\perp}$  there are also still two additional equations available which have not yet been used, one from a uniaxial tension tests and one from a fracture test with pure transverse/transverse shear stressing  $\tau_{\perp\perp}$ . This is true if the material behaves really non-intrinsically brittle.

For uniaxial transverse tension the two principal stresses at fracture are  $\sigma_{II} = 0$  and  $\sigma_{III} = R_{\perp}^t$  and for pure  $\tau_{\perp\perp}$ -stressing  $\sigma_{II} = -R_{\perp\perp}$  and  $\sigma_{III} = R_{\perp\perp}$ , see Mohr's circle in the  $(\sigma_n, \tau_{nt})$ -diagram in Figure 13c and 13b. If these strengths are inserted into the  $(\sigma_{II}, \sigma_{III})$ -fracture condition, Eq. 17, for non-intrinsic material the following two equations result, if  $R_{\perp\perp}^A$  is replaced by using Eq. 37:

$$\frac{R_{\perp}^t}{2(\sqrt{1-C_2} - p_{\perp\perp})} = \frac{R_{\perp}^c}{2(1 + p_{\perp\perp})} \quad (38)$$

$$R_{\perp\perp} \sqrt{\frac{1-C_2}{1-C_2 - (p_{\perp\perp})^2}} = \frac{R_{\perp}^c}{2(1 + p_{\perp\perp})} \quad (39)$$

$$\text{with } C_2 = \left( \frac{R_{\perp\perp}^A}{R_{\perp}^{At}} \right)^2 - 2p_{\perp\perp} \frac{R_{\perp\perp}^A}{R_{\perp}^{At}}$$

These two equations for the two still unknown values  $R_{\perp}^{At}$  and  $p_{\perp\perp}$  make it much easier now to determine  $p_{\perp\perp}$  and  $R_{\perp}^{At}$  from given data for  $R_{\perp}^t$ ,  $R_{\perp}^c$  and  $R_{\perp\perp}$  compared to the iterative procedure which we used in Part A [19] for Test Case 1. Please keep in mind that the approach described above is only applicable if an  $R_{\perp\perp}$  value has been determined by reliable experiments. In contrast to UD FRPCs this is the case for isotropic material such as the pure resin material given in Test Case 1 of the WWFE-II [19]. There, the tensile strength  $R^t$  ( $R_{\perp}^t$  in transversely isotropic notation) and the shear strength  $R^s$  ( $R_{\perp\perp}$  in transversely isotropic notation) differed significantly and the application of an approach for non-intrinsically brittle material became necessary. Using the equations 37, 38 and 39 the parameters for a non-intrinsically brittle fracture behaviour can be determined:  $R^{At}$ ,  $R^{As}$  and  $p$  ( $R_{\perp}^{At}$ ,  $R_{\perp\perp}^A$  and  $p_{\perp\perp}$  in transversely isotropic notation).

As long as no reliable experimental approaches regarding through-thickness shear are available for UD FRPCs, it is reasonable to choose  $p_{\perp\perp}$  between 0.2 and 0.3 (see Tab. 1 in [4]) and derive  $R_{\perp\perp}$  using equation 39. The result is a consistent set of parameters, both in the fracture plane-related and the original material coordinate system. For an intrinsically brittle material, the resulting  $R_{\perp\perp}$  should be close to  $R_{\perp\perp}^f$ .

## 5 Summary and Outlook

During the last two decades, numerous scientific and engineering studies revealed that failure criteria of the Mohr/Coulomb-type like the Puck IFF criteria reliably describe the physical mechanisms of inter-fibre failure in UD FRPCs. Compared to many other criteria – commonly polynomials in the space of applied stresses interpolating between experimentally accessible strengths – the Mohr/Coulomb-type criteria have the drawback of additional computational effort: the search for the fracture angle. Since 1992 [15] continuous efforts have been taken to derive analytical relations which transform the action-plane related criteria of the Mohr/Coulomb-type into the common  $(\sigma_1, \sigma_2, \sigma_3, \tau_{21}, \tau_{31}, \tau_{23})$ -stress space of applied stresses. Still this has not been achieved for a general 3D loadcase, but in addition to the available solution for the in-plane  $(\sigma_1, \sigma_2, \tau_{21})$ -stress space the present paper provides another for the  $(\sigma_1, \sigma_2, \sigma_3, \tau_{23})$ -stress space. This is a major step towards a general analytical solution. Besides the convenient determination of bearable stresses, an analytical solution also provides quick access to the fracture plane orientation and the stresses on that plane  $(\sigma_n^{\text{fr}}, \tau_{nt}^{\text{fr}}, \tau_{n1}^{\text{fr}})$  which lead to the fracture. The earlier such information is available during the design process, the more valuable is it regarding the improvement of load paths or the choice / design of material.

Regarding the Puck fracture criterion itself it is worth mentioning that no reason for any changes to the basic equations emerged over the years. Since 1996 [16] the published fracture criteria in the  $(\sigma_n^{\text{fr}}, \tau_{nt}^{\text{fr}}, \tau_{n1}^{\text{fr}})$ -stress space (see Fig. 42 in [4]) are used without any changes. While these relations inherently cover intrinsically and non-intrinsically brittle behaviour, the derivation of the analytical solutions now reveals the underlying dependencies and led to an exact definition of the term finally.

The derivation of the results is based on the Mohr's analogy between fracture mechanics and analytical geometry. This reveals another important aspect of the present work regarding isotropic material: The derived analytical solution can be understood as a comprehensive analytical description of brittle failure in isotropic materials. Here – for transversely isotropic UD FRPCs – we combined  $\sigma_2, \sigma_3$  and  $\tau_{23}$  into the principal stresses  $\sigma_{\text{II}}$  and  $\sigma_{\text{III}}$ . When applied to isotropic material,  $\sigma_{\text{II}}$  and  $\sigma_{\text{III}}$  are replaced by the major and minor principal stress (see Sec. 4.2.5.1 in [4]).

The basic ideas of the Puck theory were published back in 1992 [15] and in the beginning the method of approach hesitantly gained acceptance as it significantly differs from common global stress approaches. While the lack of literature impeded the access to the theory in the beginning, nowadays the theory is well documented and the number of users and supporters increased considerably. The theory including the extension and development which are currently ready to use are described in the

comprehensive textbook written by Knops [4] and several computer programs and FE material subroutines are provided for purchase or download [22-24]. On the scientific level, a comprehensive ABAQUS-implementation has been described in [19, 20]. Finally, it is worth mentioning that the capabilities of the Puck theory have been proven in the WWFE-I [17, 18] and WWFE-II [11, 19]. The latter includes a comparison with eleven different criteria and provides an extensive overview on current approaches in UD FRPC failure prediction.

## **Acknowledgement**

The present results have been achieved during the author's participation in the World Wide Failure Exercise II (WWFE-II) and have been reviewed in the context of the Part A and Part B paper publication [11,19]. However, the analytical solutions are not closely related to the twelve test cases of the WWFE-II. Thus, we suggested to publish them online on the author's website [25]. This idea has been strongly supported by Dr. Kaddour, one of the organizers of the WWFE-II. We gratefully acknowledge his agreement and the interesting scientific discussions with him. The present work has neither been funded by any public, commercial or private source. It has been accomplished during leisure of the authors and the understanding and support of the families and surrounding has been highly appreciated. The readers are kindly invited to contact the authors in the case of any questions.

For beginners in the field of Coulomb-Mohr-type fracture criteria the book of M. Knops [4] is highly recommended whereas the 2D-stress calculation tool developed by TU Darmstadt [24] provides further insight from the practical aspect.

## References

1. J. Göswein, Technology and first operational results of the world's largest offshore wind turbine REPOWER 6M. Proceedings of the European offshore wind conference 2009. <http://www.offshorewind2009.info>.
2. G. Marsh, Composites lift off in primary aerostructures, Reinforced Plastics, vol.48 no.4, pp.22-27, 2004.
3. M.J. Hinton, A.S. Kaddour, P.D. Soden (Eds.), Failure Criteria in Fibre Reinforced Polymer Composites: The World-Wide Failure Exercise, Elsevier, Amsterdam, 2004.
4. M. Knops, Analysis of Failure in Fiber Polymer Laminates: The Theory of Alfred Puck, Springer, Berlin, 2008.
5. Puck, Einige Beispiele zu Konstruktion und Bau von hochbeanspruchten Segelflugzeugteilen aus Glasfaserkunststoff, Schweizer Aero-Revue, Zurich, 37 (1962) pp. 713-717, 38 (1963) pp. 35-42 (Some examples of design and construction of high load sailplane components of GFRP) (German).
6. Segelfliegen: Stabiler als Stahl(Gliding: Stronger than steel), Der Spiegel 31/1978, available online at <http://www.spiegel.de/spiegel/print/d-40606617.html> (accessed April 22, 2013).
7. Puck, Dimensionierung tragender Leichtbaukonstruktionen aus Glasfaser-Kunststoffen, Kunststoffe 53 (1963), pp. 150–157.(dimensioning of load carrying light weight components of GFRP) (German) .
8. Puck, H. Wurtinger, Werkstoffgemäße Dimensionierungs-Größen für den Entwurf von Bauteilen aus kunstharzgebundenen Glasfasern, Forschungsberichte des Landes Nordrhein-Westfalen Nr. 1253, Köln u. Opladen Westdeutscher Verlag 1963. (Special material properties for the design of GFRP-components) (German).
9. Puck, W. Schneider, On failure mechanisms and failure criteria of filament-wound glass-fibre/resin composites. Plastics and Polymers February 1969, The Plastics Institute Transactions and Journal, Pergamon press, pp: 33-44.
10. Puck, Festigkeitsberechnung an Glasfaser/Kunststoff-Laminaten bei zusammengesetzter Beanspruchung; Bruchhypothesen und schichtweise Bruchanalyse (Strength analysis on GRP laminates under combined stresses; fracture hypotheses and layer by-layer failure analysis), Kunststoffe, German Plastics 59 (bilingual edition English and German), (1969), pp 18-19, German text pp 780-787.
11. H. Matthias Deuschle, Alfred Puck, Application of the Puck Failure Theory for Fibre Reinforced Composites under 3D-Stress: Comparison with Experimental Results, Journal of Composite Materials, vol.47(6-7), pp.827-846, 2013.
12. M. Mannigel, Influence of Shear Stresses on the Fibre Failure Behaviour in CarbonFibre Reinforced Plastics (CFRP), PhD Thesis, Institut für Kunststoffverarbeitung (IKV), RWTH Aachen, 2007 [German].
13. C.A. Coulomb, Sur une Application des Règles de Maximis et Minimis a quelques Problemes de Statique relatives a l'Architecture, in: Memoires de Mathematique et de Physique: Ann´e 1773, Academie Royal des Sciences par divers Savans, Paris, France, 1776 [French].
14. Mohr, Welche Umstände bedingen die Elastizitätsgrenze und den Bruch eines Materials, Zeitschrift des VDI, vol.24 no.45&46, pp.1524-1541 & 1572-1577, 1900 [German].
15. Puck, A failure criterion shows the direction, Kunststoffe - German Plastics, vol.82, pp.29-32, 1992 [German and English].

16. Puck, Festigkeitsanalyse von Faser-Matrix-Laminaten: Modelle für die Praxis, Hanser Verlag, München, 1996 [German] available online at [http://www.klub.tu-darmstadt.de/forschungsbericht/downloads\\_3/downloads\\_3.de.jsp](http://www.klub.tu-darmstadt.de/forschungsbericht/downloads_3/downloads_3.de.jsp) (accessed April 22, 2013).
17. Puck, H. Schürmann, Failure analysis of FRP laminates by means of physically based phenomenological models, Composites Science and Technology, vol.58 no.7, pp.1045-1067, 1998.
18. Puck, H. Schürmann, Failure analysis of FRP laminates by means of physically based phenomenological models, Composites Science and Technology, vol.62 no.12- 13, pp.1633-1662, 2002.
19. H. Matthias Deuschle, Bernd-H. Kröplin, FE Implementation of Puck's Failure Theory for Fibre Reinforced Composites under 3D-Stress, Journal of Composite Materials, vol.46(19-20), pp.2485-2513, 2012.
20. H. Matthias Deuschle, 3D Failure Analysis of UD Fibre Reinforced Composites: Puck's Theory within FEA, PhD Thesis, ISD, Universität Stuttgart, 2010.
21. Paul, A Modification of the Coulomb-Mohr Theory of Fracture, Journal of Applied Mechanics, vol.28, pp.259-268, 1961.
22. Tobias Kremer, KLuB-VDI2014 v2.0: Subroutine zur Festigkeitsanalyse von Faser-Kunststoff-Verbunden nach der VDI-Richtlinie 2014, Teil 3 für ABAQUS, Fachgebiet Konstruktiver Leichtbau und Bauweisen (KLuB), TU Darmstadt, 2007, available online at [http://www.klub.tu-darmstadt.de/forschungsbericht/downloads\\_3/downloads\\_3.de.jsp](http://www.klub.tu-darmstadt.de/forschungsbericht/downloads_3/downloads_3.de.jsp) (accessed April 22, 2013)
23. Compositor 3.0: Steifigkeits- und Festigkeitsanalyse von mehrschichtigen Laminaten aus Faserverbundkunststoffen (FVK), Institut für Kunststoffverarbeitung (IKV), RWTH Aachen, 2010
24. AlfaLam\_nl VDI2014: Berechnungstool zur nichtlinearen Laminatanalyse nach der VDI 2014, Fachgebiet Konstruktiver Leichtbau und Bauweisen (KLuB), TU Darmstadt, 2010, available online at [http://www.klub.tu-darmstadt.de/forschungsbericht/downloads\\_3/downloads\\_3.de.jsp](http://www.klub.tu-darmstadt.de/forschungsbericht/downloads_3/downloads_3.de.jsp) (accessed April 22, 2013)
25. [www.alfredpuck.de](http://www.alfredpuck.de) (accessed April 22, 2013)